NACA RM L56D10

NACA

RESEARCH MEMORANDUM

LONGITUDINAL STABILITY CHARACTERISTICS OF A SIMPLE INFRARED HOMING MISSILE CONFIGURATION AT MACH NUMBERS OF 0.7 TO 1.4

By Clarence A. Brown, Jr.

Langley Aeronautical Laboratory
Langley Field, Va.

NATIONAL ADVISORY COMMITTEE
FOR AERONAUTICS

WASHINGTON
June 12, 1956
Declassified September 11, 1959

NACA RM L56D10

NATIONAL ADVISORY COMMITTEE FOR AERONAUTICS

RESEARCH MEMORANDUM

LONGITUDINAL STABILITY CHARACTERISTICS OF A SIMPLE INFRARED HOMING MISSILE CONFIGURATION AT MACH NUMBERS OF 0.7 TO 1.4

By Clarence A. Brown, Jr.

SUMMARY

The longitudinal stability characteristics of a simple infrared homing missile have been determined in flight with a rocket-powered model by the Langley Pilotless Aircraft Research Division. Static and dynamic longitudinal stability derivatives of this cruciform, interdigitated, canard-wing missile configuration were determined from an investigation using the pulse-rocket technique for a Mach number range of 0.7 to 1.4.

The average lift-curve slope for the model varied smoothly over the Mach number range tested. The large tail length of the model was extremely effective in increasing the damping-in-pitch derivative throughout the Mach number range tested but the damping, in terms of percent critical damping, was approximately 10 to 20 percent because of the large inertia of the model. The aerodynamic-center location varied smoothly with Mach number with the most forward location occurring near a Mach number of 1.0. The maximum shift in the aerodynamic-center location occurred between a Mach number of 1.0 and 1.35. This shift was approximately 9.0 inches (1.8 body diameters).

INTRODUCTION

The accuracy of present-day aircraft rocket armament has been hampered by launching errors, random dispersions, missile reliability, and missile complexity. The accuracy might be improved by incorporating some type of homing device that would reduce these errors and dispersions. An investigation has been undertaken to develop a simple infrared homing system that would be reliable as well as rugged. Such a homing system has been developed and is described in references 1 and 2. The basic idea of this system involves the use of aerodynamics to help in reducing homing-system complications and aid in increasing missile reliability. This was

accomplished by using a flicker control to produce roll which operates directly from the target position as a primary reference, by using a rotating lift vector, and by using the rolling of the missile to scan the seeker field of view.

This paper presents the results from a flight-test investigation, using the pulse-rocket technique, to determine the static and dynamic longitudinal stability derivatives and the drag data for a missile configuration similar to the one reported in reference 2. The Mach number range covered by this investigation was approximately 0.7 to 1.4. The model used in this investigation was flight tested at the Langley Pilotless Aircraft Research Station at Wallops Island, Va.

SYMBOLS

All coefficients are based on a body diameter of 5 inches (0.416 foot) and a body cross-sectional area of 0.1363 square foot.

a_n/g normal-accelerometer reading, g units

a_l/g longitudinal-accelerometer reading, g units

a_t/g transverse-accelerometer reading, g units

b exponential damping constant, e^{-bt}, per second

d body diameter, 0.416 ft

g acceleration due to gravity, ft/sec^2

q dynamic pressure, lb/sq ft

C_D drag coefficient, $\left(-\frac{a_l}{g}\cos\alpha + \frac{a_n}{g}\sin\alpha\right)\frac{W}{qA_b}$

$C_{D_{min}}$ minimum drag coefficient

C_L lift coefficient, $\left(\frac{a_n}{g}\cos\alpha + \frac{a_l}{g}\sin\alpha\right)\frac{W}{qA_b}$

C_m pitching-moment coefficient, $\frac{\text{Pitching moment about center of gravity}}{qA_b d}$

C_N normal-force coefficient, $\frac{a_n}{g}\frac{W}{qA_b}$

C_Y lateral-force coefficient, $\frac{a_t}{g}\frac{W}{qA_b}$

C_R resultant-force coefficient corrected for trim, $\left[\left(C_N - C_{N_{trim}}\right)^2 + \left(C_Y - C_{Y_{trim}}\right)^2\right]^{1/2}$ (Note that subscript "trim" denotes trim values of model during rolling.)

M Mach number

P period of oscillation, sec

t time, sec

R Reynolds number

A_b body cross-sectional area at wing-body juncture, 0.1363 sq ft

V velocity of model, ft/sec

W model weight, lb

α angle of attack, deg

$\dot{\alpha} = \frac{1}{57.3}\frac{d\alpha}{dt}$, radians/sec

$\dot{\theta}$ pitching velocity, radians/sec

$\dot{\phi}$ rolling velocity, radians/sec

$C_{L_\alpha} = \frac{\partial C_L}{\partial \alpha}$, per degree

$C_{m_\alpha} = \frac{\partial C_m}{\partial \alpha}$, per degree

$$C_{m_q} = \frac{\partial C_m}{\partial \frac{\dot{\theta} d}{2V}}, \text{ per radian}$$

$$C_{m_{\dot{\alpha}}} = \frac{\partial C_m}{\partial \frac{\dot{\alpha} d}{2V}}, \text{ per radian}$$

MODEL AND APPARTUS

Model Description

Sketches of the rocket-powered model used in this test are shown in figure 1. Sketches of the control surface and wing surface are shown in figure 2. Photographs of the model and model-booster combination are shown in figures 3 and 4, respectively. Physical characteristics determined by preflight measurements are presented in table I.

The body of the model consisted of two cylindrical sections 5.0 and 5.5 inches in diameter, and had a body-length—maximum-diameter ratio of 24.58 (fig. 1). The 5.0-inch-diameter section was a modified HPAG rocket motor. The nose consisted of a flat face with a drag-reducing conical windshield. The conical windshield was supported by an octapod mounted in front of the flat nose. Protruding in front of the conical windshield was a sting used to mount the angle-of-attack indicator (figs. 1 and 3). The canard surfaces were mounted on the 5.5-inch-diameter cylindrical section of the body, were of tapered plan form, and had a maximum thickness at the wing-body juncture of 5.1 percent of the chord (fig. 2). The canard surfaces in the horizontal plane were fixed at an angle of incidence of 3.93° and the canard surfaces in the vertical plane were fixed at zero angle of incidence.

The 60° delta cruciform wings were mounted on the 5-inch-diameter cylindrical section of the body and were interdigitated 45° to the canard surfaces. The wing had a modified hexagonal airfoil section with a constant thickness corresponding to a thickness of 1.4 percent of the chord at the wing-body juncture.

The model used in this investigation differed from the model of reference 2 as follows:

(1) An angle-of-attack indicator was added ahead of the conical windshield.

(2) The front end of the model was fixed to the rear section of the model in such a manner as to eliminate the rolling of the front section with respect to the rear section.

(3) The 5.5-inch-diameter section of the fuselage was lengthened by 10 inches but the model overall length was not changed.

(4) The tracking flares placed on two of the rear fins were eliminated.

Instrumentation

The model was equipped with an NACA six-channel telemeter which transmitted a continuous record of normal, transverse, and longitudinal accelerations; angle of attack; total pressure; and rate of roll. The transverse, longitudinal, and normal accelerometers were located so as to be near the center of gravity of the model when the sustainer motor had burned out. Angle of attack was measured by a free-floating vane mounted on a sting which protruded ahead of the drag-reducing conical windshield (figs. 1 and 3). Total pressure was obtained by a total-pressure tube extended from the fuselage ahead of the wings and in a plane $22\frac{1}{2}^{\circ}$ to the main wing and canard surfaces. The rate-of-roll instrument was located just ahead of the center of gravity of the model when the sustainer had burned out.

Model velocity was obtained from the CW Doppler velocimeter and the model trajectory was determined through use of a NACA modified SCR 584 radar tracking unit. A radiosonde, released at the time of flight, was used to obtain atmospheric data throughout the altitude range traversed by the model.

Test Technique

The model was launched at 58° 17' elevation angle from a zero-length launcher as shown in figure 4. The model was boosted to a Mach number of 0.7 by a modified HVAR rocket motor which delivered approximately 7,000 pounds of thrust for 1.0 second. After separation from the booster, a sustainer motor, made as an integral part of the model, delivered approximately 2,500 pounds of thrust for 2.6 seconds and propelled the model to the peak Mach number of 1.54. After the sustainer burnout, the model was disturbed in pitch by a series of six small rocket motors providing thrust normal to the longitudinal axis of the model and located near the nose of the model. These rocket motors were timed to fire in sequence during the decelerating portion of the flight. Transient

responses of the resulting disturbances of the model were continuously recorded in the form of time histories as the model decelerated through the Mach number range. The methods for obtaining the longitudinal stability data from the transient responses are presented in references 3 and 4.

PRECISION OF DATA

Correction

The velocity data, as obtained by the CW Doppler velocimeter, were corrected for flight-path curvature and wind effects at altitude. The magnitudes and direction of these winds were determined by tracking the radiosonde balloon.

In order to obtain the angle of attack at the center of gravity of the model, the angle of attack measured at the nose was corrected for model pitching velocity and flight-path curvature by the method presented in reference 5.

Accuracy

It is believed that the absolute accuracy of the quantities, based on the accuracy of the model and ground-instrumentation calibration, are within the values tabulated in the following table for two Mach numbers: (The magnitude of the random error can be seen by the scatter of the points on the curves.)

M	Limit of accuracy of -*				
	M	α, deg	C_L	$C_{D_{min}}$	C_Y
0.80	0.01	0.50	0.26	0.13	0.10
1.35	.01	.50	.12	.07	.04

*These values may be positive or negative depending on the model and ground-instrumentation zero calibration.

Parameters dependent upon differences in measured quantities or slopes such as C_{L_α} are much more accurately determined than the previously mentioned errors would indicate.

RESULTS AND DISCUSSION

Data were received for the model tested for a Mach number range of 0.75 to 1.40. The Reynolds number of this test ranged from approximately 4×10^6 to 9×10^6, per foot. Variation of Reynolds number with Mach number for the test is shown in figure 5.

Time histories of the lift coefficient C_L, lateral-force coefficient C_Y, rolling velocity $\dot{\phi}$, and Mach number are presented in figure 6. Although the model had no controls to produce rolling of the model or a roll-control system to prevent rolling, figure 6 shows that as the sustainer motor burned out (4.7 seconds), the roll rate of the model exceeded the instrumentation limit of 10 radians per second. As the Mach number decreased (increased time), the roll rate became less and at a Mach number of 0.75 the roll rate of the model was near zero. As may be noted in figure 6, irregularities in C_L and C_Y occurred during the flight of the model. These irregularities of C_L and C_Y are due to the rolling of the model since the disturbing force occurred only in the pitch plane. The irregularities of the lift coefficient made it impossible to obtain the model period or the exponential damping constant by the direct analysis of the time histories of the lift coefficient.

In order to obtain the period and the exponential damping constant of the model, it was necessary to analyze the time histories of the resultant-force coefficient by the method presented in reference 4. This method consisted of plotting C_N against C_Y for each of the pulse-rocket disturbances and, after accounting for the trim as well as possible, developing time histories of C_R. A typical plot of the time history of resultant-force coefficient is presented in figure 7.

Lift Coefficient

Plots of lift coefficient against angle of attack are shown in figure 8 for various Mach numbers. The lift coefficient against angle of attack showed some nonlinearities; however, not enough data were available to determine any consistent variation with angle of attack. Since angle of sideslip was not measured on this model, it was not possible to make plots of C_Y against β or C_R against resultant angle.

Presented in figure 9 is the variation of average lift-curve slope with Mach number. The lift-curve slope was linear within the limits of the data and varied smoothly with Mach number over the entire Mach number range tested.

Dynamic Stability

The exponential damping constant b is presented in figure 10 for the model tested. The rolling of the model and the interaction of the normal and transverse motions made it necessary to obtain the exponential damping constant from the time histories of resultant-force coefficient rather than from the angle-of-attack or normal-acceleration traces. The method of obtaining the exponential damping constant is presented in reference 4. Some of the scatter in b can probably be attributed to the irregularities in trim which were caused by the rolling motions.

The damping-in-pitch derivative $C_{m_q} + C_{m_{\dot{\alpha}}}$ was obtained from the faired values of b (fig. 10) and the faired values of C_{L_α} (fig. 9) and is presented as a function of Mach number in figure 11. Unpublished data for a similar high-fineness-ratio missile configuration show that the damping-in-pitch derivative $C_{m_q} + C_{m_{\dot{\alpha}}}$ was of the same order of magnitude as that of the present test. The value of $C_{m_q} + C_{m_{\dot{\alpha}}}$ for the present test is about 10 times that for the model of reference 4 which had about the same ratio of body cross-sectional area to wing area.

For the Mach number range tested, the large tail length was extremely effective in increasing the damping-in-pitch derivative $C_{m_q} + C_{m_{\dot{\alpha}}}$ but the damping, in terms of percent critical damping, was approximately 10 to 20 percent because of the large inertia of the model.

Static Stability

The longitudinal period of oscillation of the model obtained by using the time histories of the resultant-force coefficient is presented in figure 12 as a function of Mach number. The pitching-moment derivative C_{m_α} was obtained from the faired values of the period of oscillation of the model $\left(\text{assuming } C_m \text{ linear with } \alpha\right)$ and is presented in figure 13 as a function of Mach number. The pitching-moment derivative (fig. 13) was nearly constant throughout the test Mach number range. Preliminary estimates indicated that the pitching moment would be greater at supersonic speeds than at subsonic speeds. Some of this difference between estimates and flight data may be attributed to the influence of the flat nose on the body of the model.

Aerodynamic-center location was determined from the C_{m_α} curve and the faired values of C_{L_α} and is presented in figure 14 in terms of inches from station 0 against Mach number. Also included in figure 14 are the

center-of-gravity locations of the model with sustainer loaded and empty. The aerodynamic center moved toward the nose of the model as the Mach number increased from 0.75 to 1.0 and then started a gradual rearward movement with increased Mach number. This rearward movement resulted in a maximum shift of 9 inches (1.8 body diameters) between a Mach number of 1.0 and a Mach number of 1.35. The aerodynamic-center location did not appear to have been affected by the rolling of the model.

Drag

Drag data for the model tested is presented in the form of $C_{D_{min}}$, based on the fuselage cross-sectional area, against Mach number in figure 15. The drag polars for this model were obtained while the transverse acceleration was near zero; therefore, no appreciable drag occurred due to angle of sideslip. As may be seen in figure 15, the values of $C_{D_{min}}$ are large, but for a configuration such as this these values appear to be reasonable. The configuration used in this test was not an optimum configuration for drag. As stated in reference 2 this configuration was chosen in order to use standard components, to have simplicity in operation, and to keep development cost and tests to a minimum.

CONCLUSIONS

The results of a flight investigation of a simple infrared homing missile configuration for a Mach number range of 0.7 to 1.4 indicated the following conclusions:

1. The average lift-curve slope for the model tested varied smoothly with Mach number over the entire Mach number range.

2. The tests indicates that the large tail length of the model was extremely effective in increasing the damping-in-pitch derivative throughout the Mach number range tested but the damping, in terms of percent critical damping, was approximately 10 to 20 percent because of the large inertia of the model.

3. The aerodynamic-center location varied smoothly with Mach number with the most forward location occurring near a Mach number of 1.0. The maximum shift in the aerodynamic-center location occurred between a Mach number of 1.0 and 1.35. This shift was approximately 9.0 inches (1.8 body diameters).

Langley Aeronautical Laboratory,
National Advisory Committee for Aeronautics,
Langley Field, Va., April 5, 1956.

REFERENCES

1. Gardiner, Robert A.: A Combined Aerodynamic and Guidance Approach for a Simple Homing System. NACA RM L53I10a, 1953.

2. Gardiner, Robert A., Gillis, Clarence L., and Graves, G. B., Jr.: Analysis of a Flight Investigation at Supersonic Speeds of a Simple Homing System. NACA RM L55J28, 1956.

3. Niewald, Roy J., and Moul, Martin T.: The Longitudinal Stability, Control Effectiveness, and Control Hinge-Moment Characteristics Obtained From a Flight Investigation of a Canard Missile Configuration at Transonic and Supersonic Speeds. NACA RM L50I27, 1950.

4. Baber, Hal T., Jr., and Moul, Martin T.: Longitudinal Stability and Control Characteristics As Determined by the Rocket-Model Technique for an Inline, Cruciform, Canard Missile Configuration With a Low-Aspect-Ratio Wing Having Trailing-Edge Flap Controls for a Mach Number Range of 0.7 to 1.8. NACA RM L54B12, 1955.

5. Ikard, Wallace L.: An Air-Flow-Direction Pickup Suitable for Telemetering Use on Pilotless Aircraft. NACA RM L53K16, 1954.

TABLE I

PHYSICAL CHARACTERISTICS DETERMINED BY PREFLIGHT MEASUREMENTS

Wing:	
Total wing area in one plane including body intercept, sq ft	2.00
Wing mean aerodynamic chord, ft	1.24
Thickness-chord ratio at body juncture	0.014
Wing span, ft	2.15
Leading-edge sweep, deg	60
Canard control surfaces:	
Exposed canard area in one plane, sq ft	0.311
Exposed canard mean aerodynamic chord, ft	0.481
Thickness-chord ratio at body juncture	0.051
Control-surface span, ft	1.125
General:	
Maximum body diameter, in.	5.5
Body diameter at wing-body juncture, in.	5.0
Fineness ratio	24.58
Maximum body cross-sectional area, sq ft	0.165
Body cross-sectional area at wing-body juncture, sq ft	0.1363
Weight, model sustainer loaded, lb	158.5
Weight, model sustainer empty, lb	116.5
Moment of inertia -	
I_Y, model sustainer empty, slug-ft^2	44.72
I_X, model sustainer empty, slug-ft^2	0.20
Center-of-gravity location, model sustainer empty, in. from nose	69.99
Center-of-gravity location, model sustainer loaded, in. from nose	76.88
Ratio of span of control surfaces to span of wings	0.52

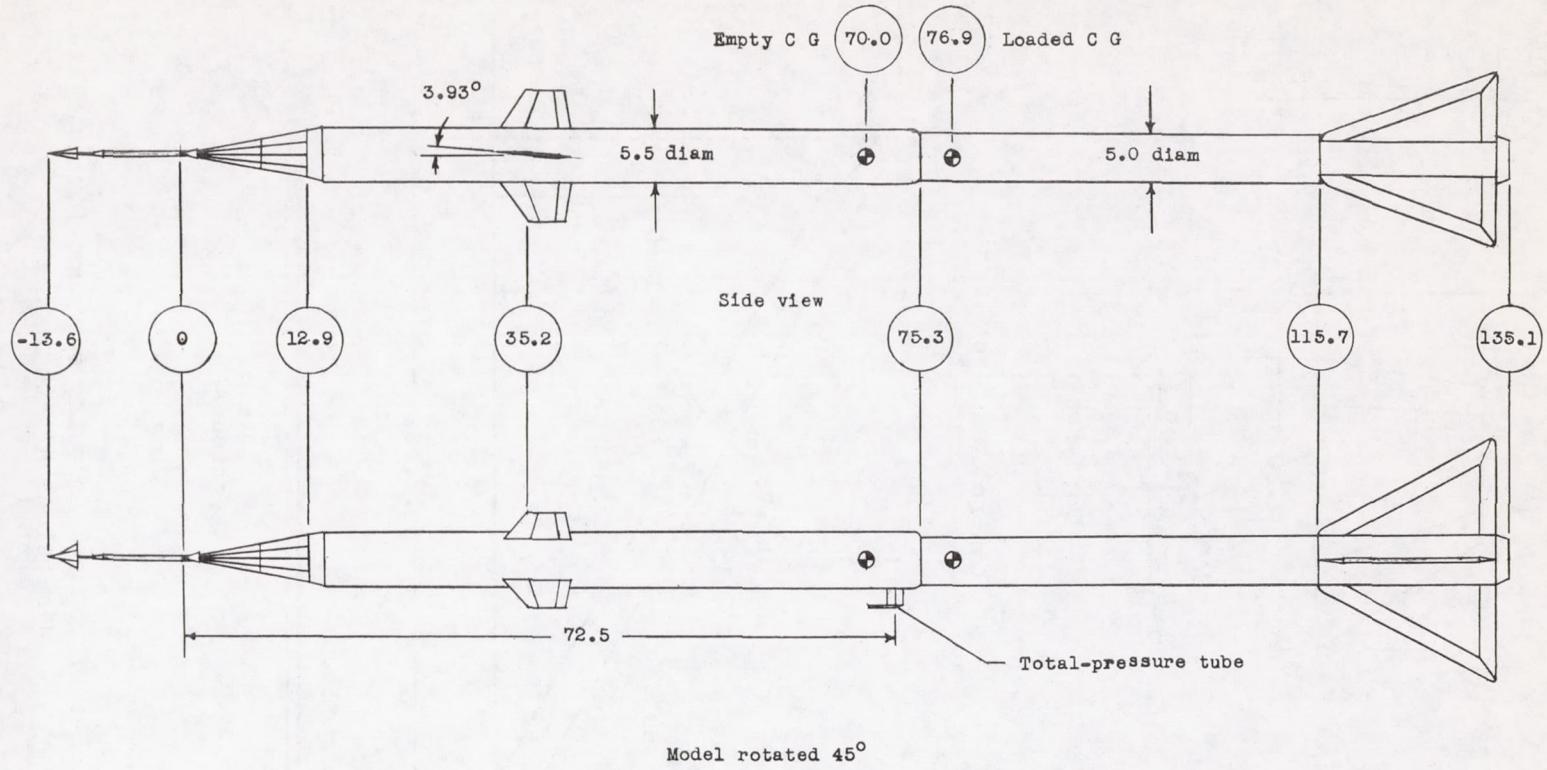

Figure 1.- Sketches of model tested. All dimensions are in inches.

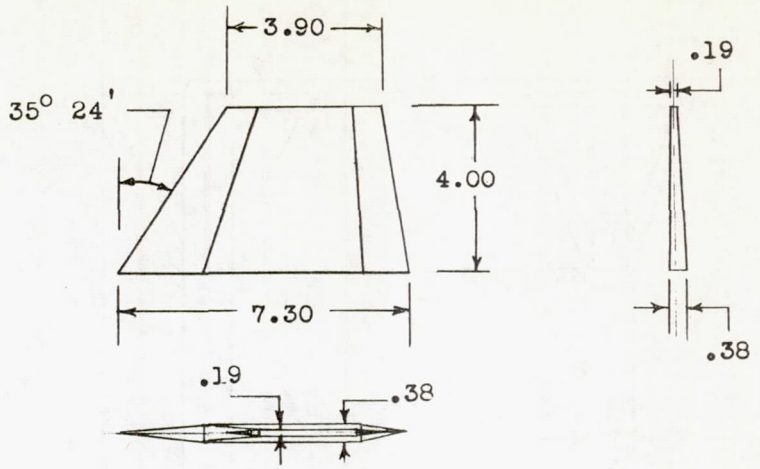

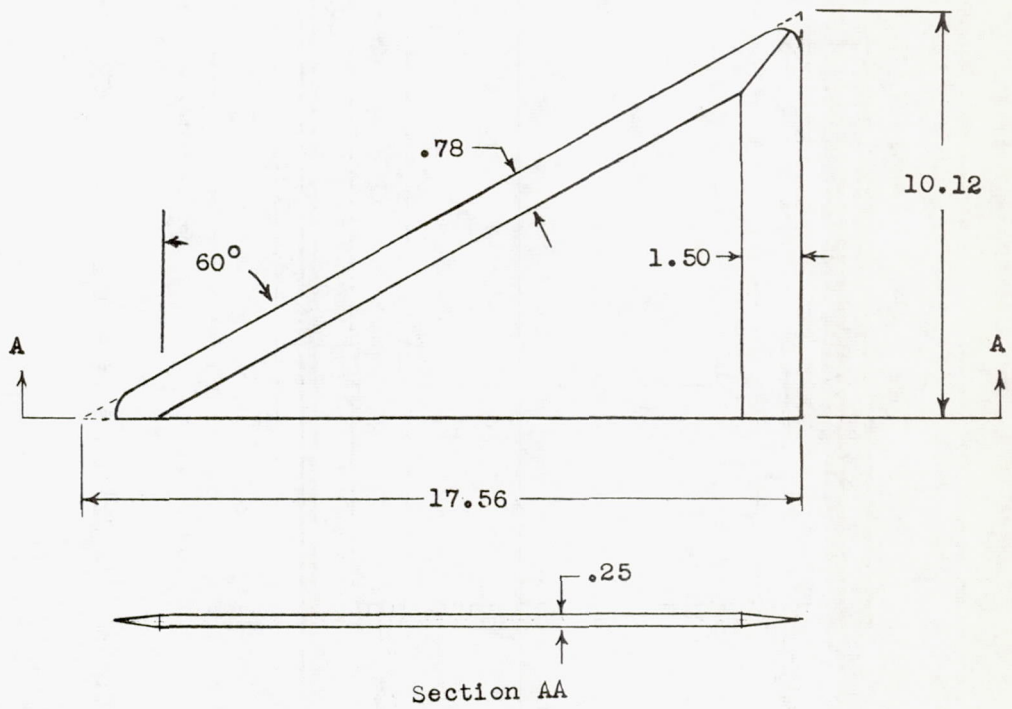

Figure 2.- Sketches of control and wing surfaces for model tested. All dimensions are in inches.

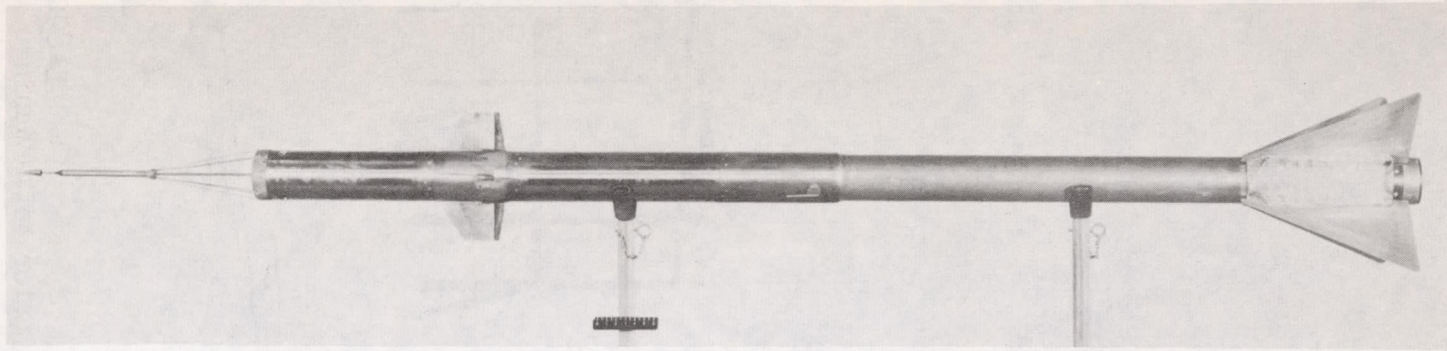

Side view L-88491.1

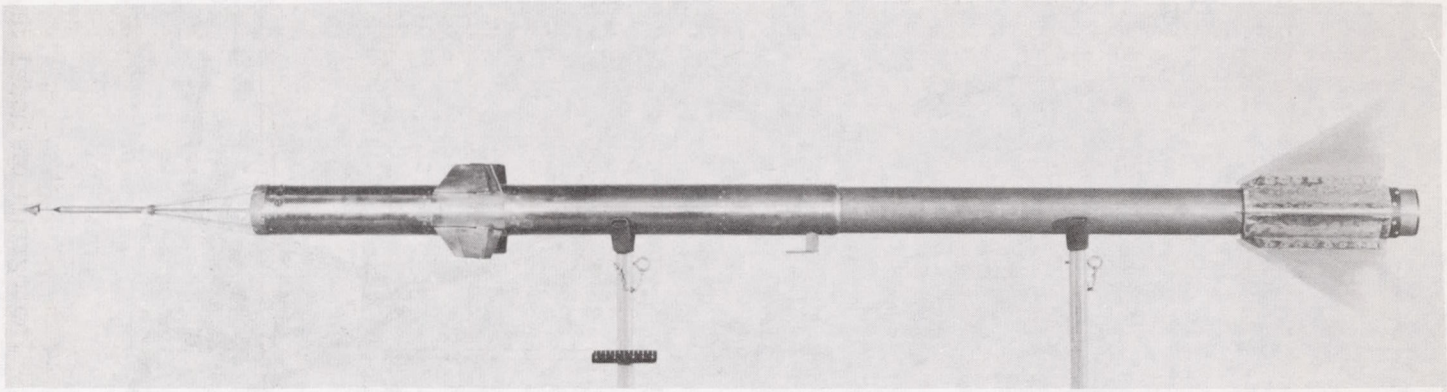

Model rotated 45° L-88490.1

Figure 3.- Photographs of model tested.

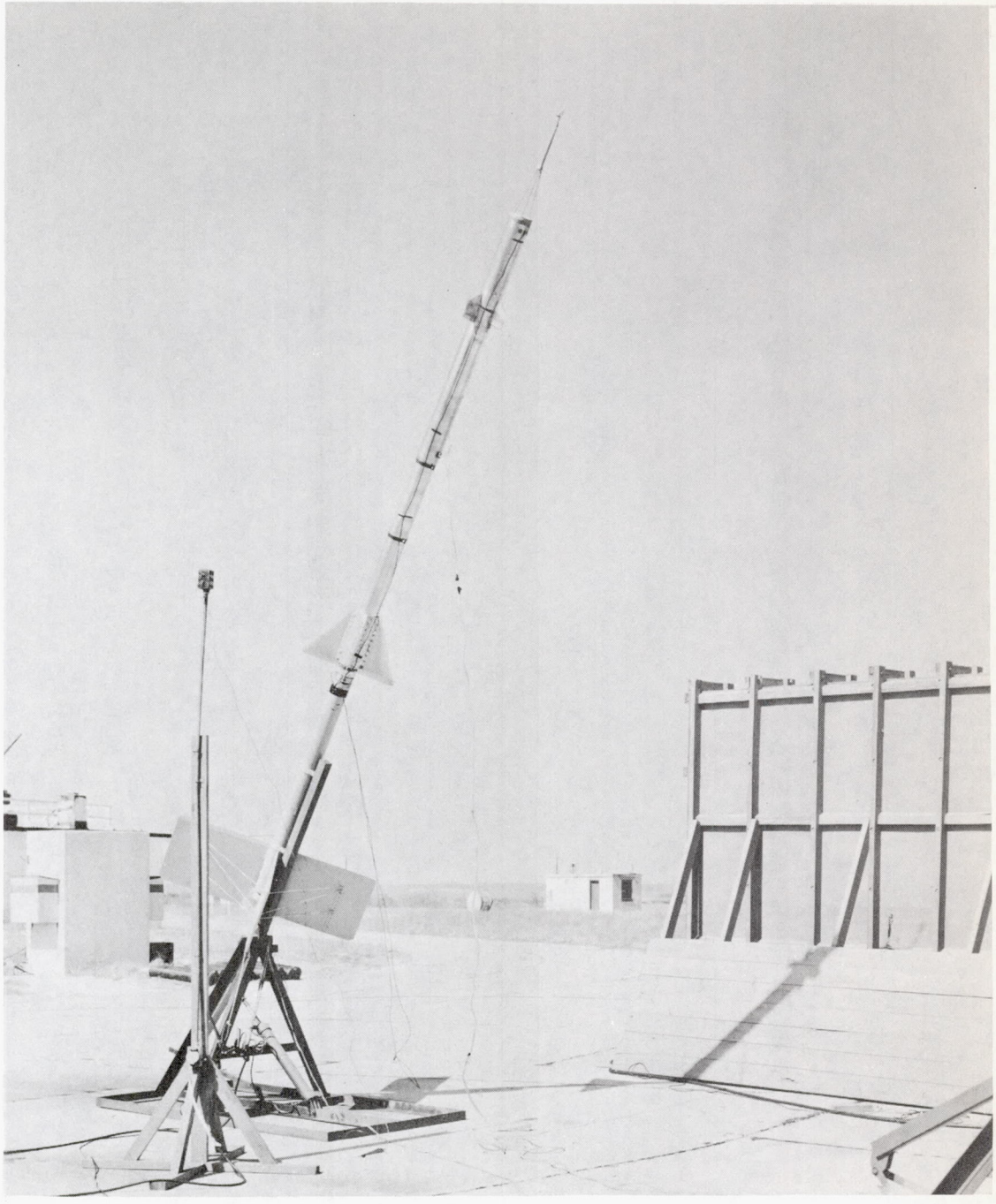

L-89036

Figure 4.- Photograph of model and booster prior to launching.

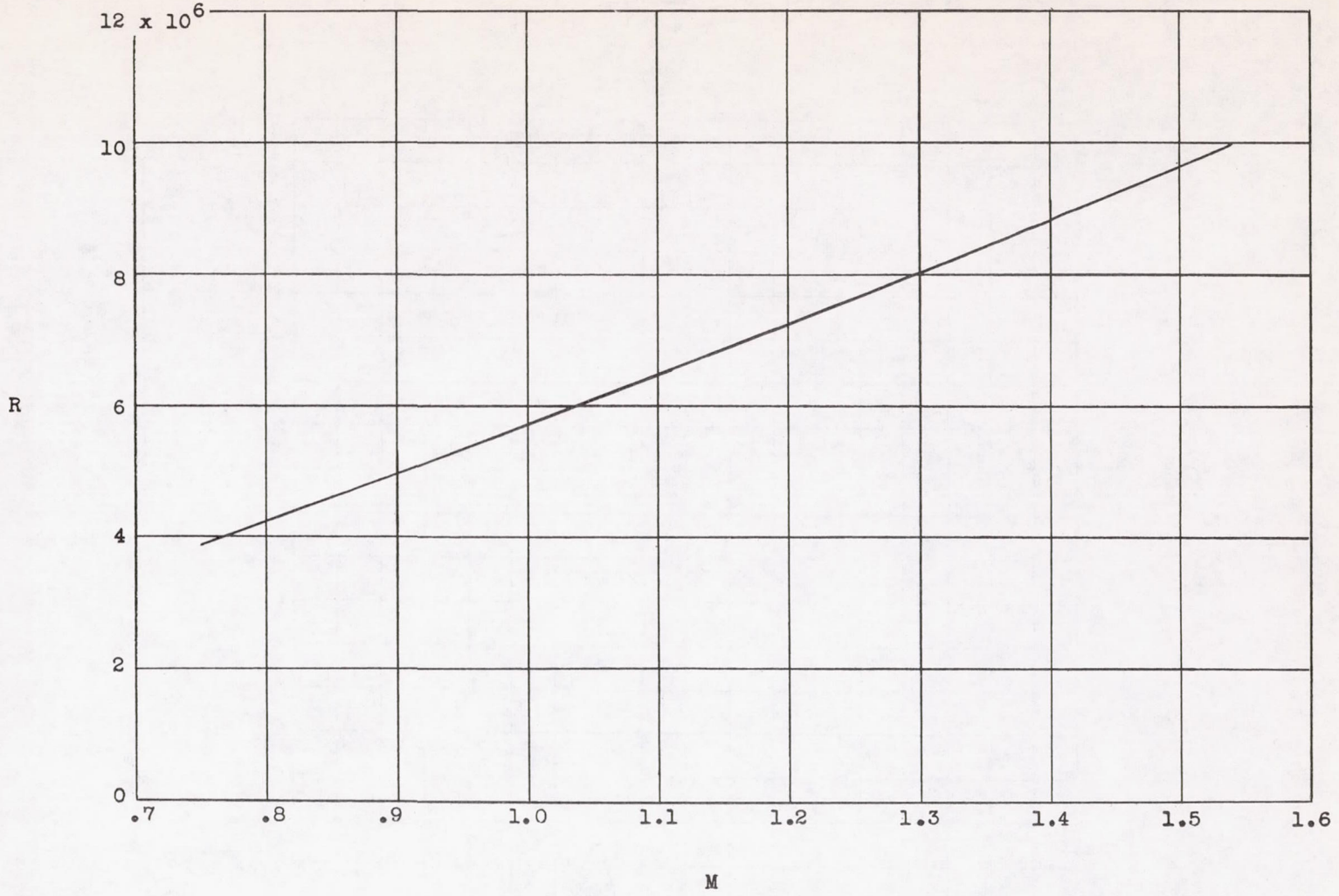

Figure 5.- Variation of Reynolds number, per foot, with Mach number.

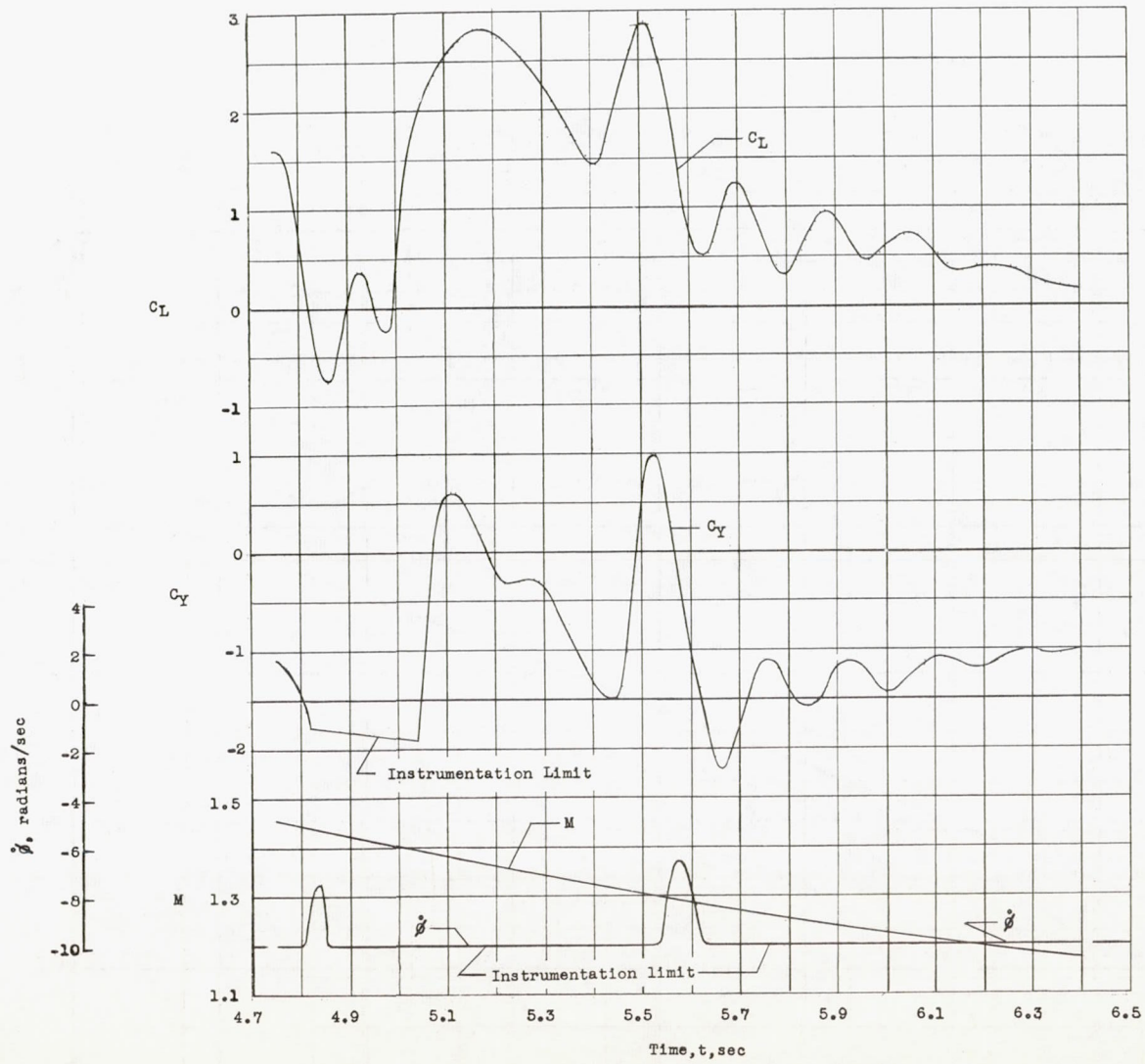

Figure 6.- Time histories of model tested.

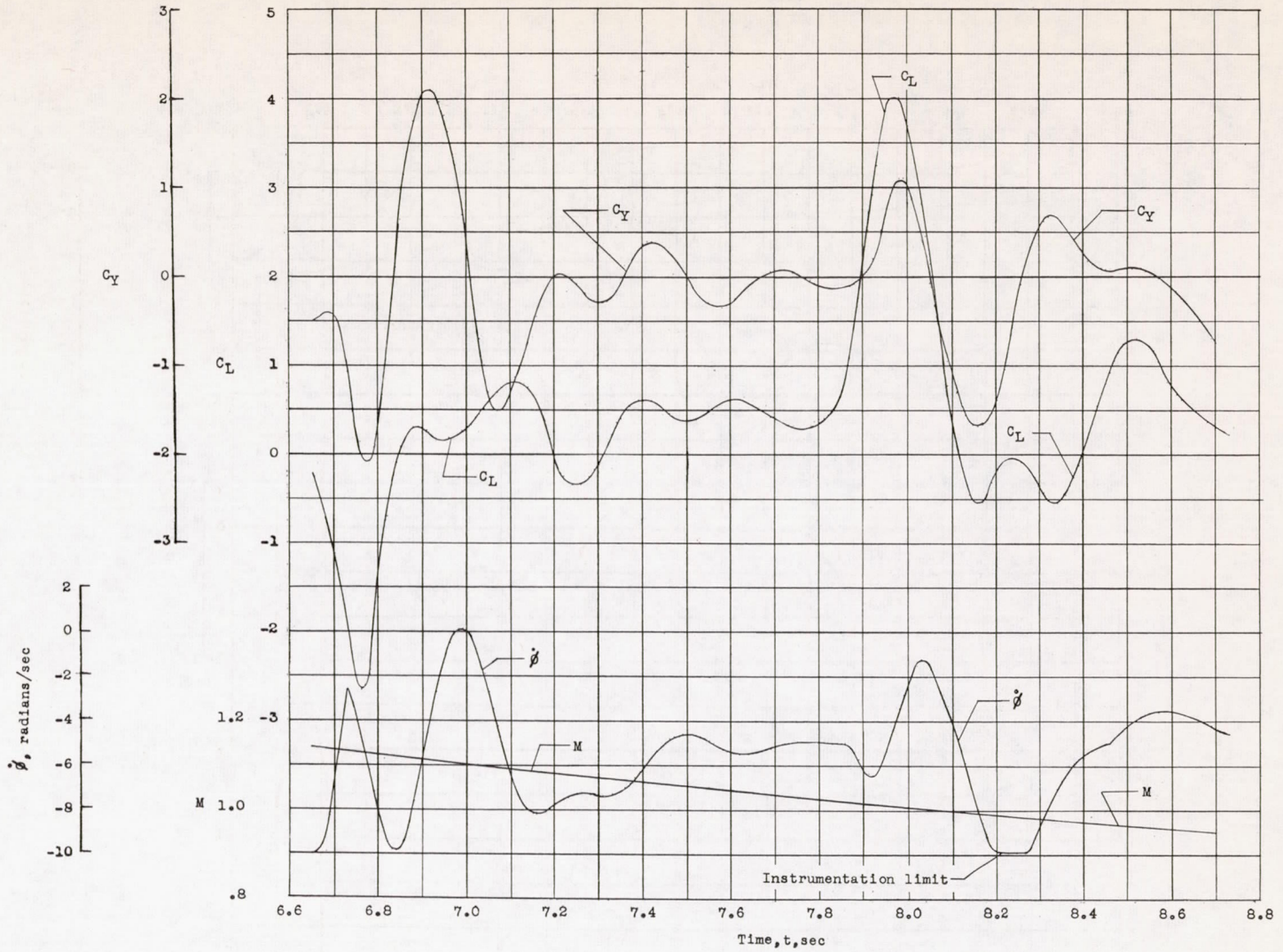

Figure 6.- Continued.

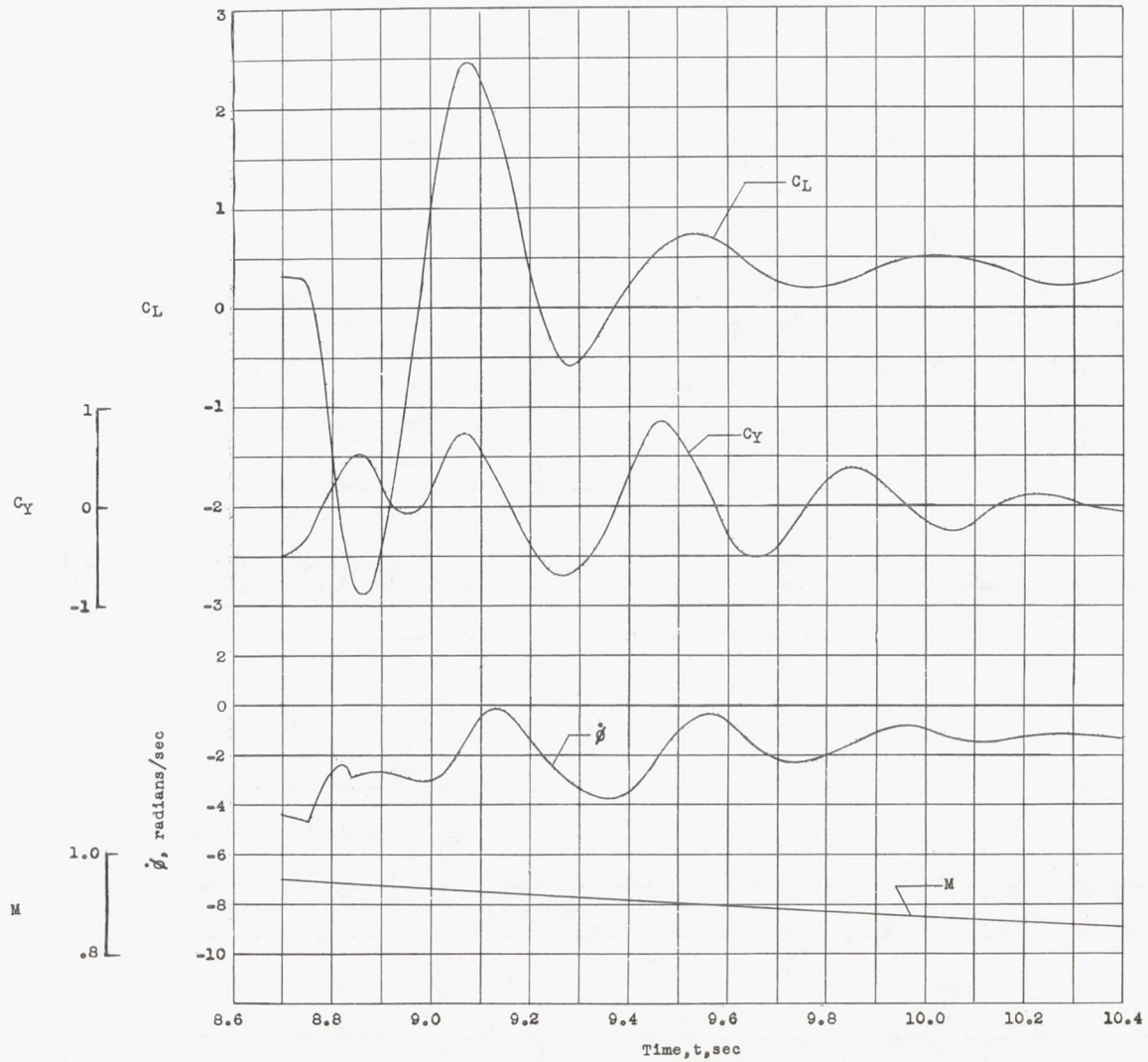

Figure 6.- Continued.

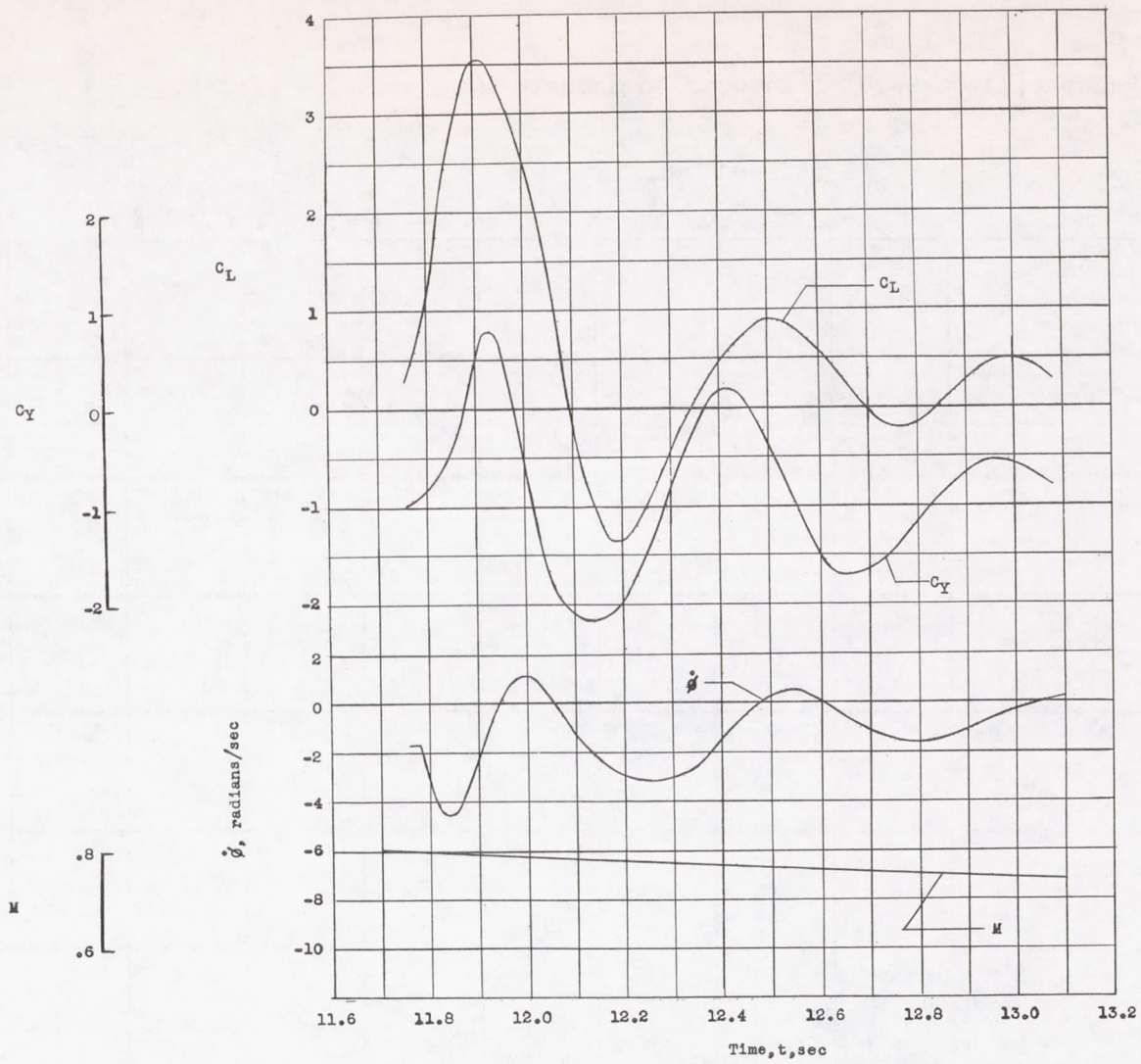

Figure 6.- Concluded.

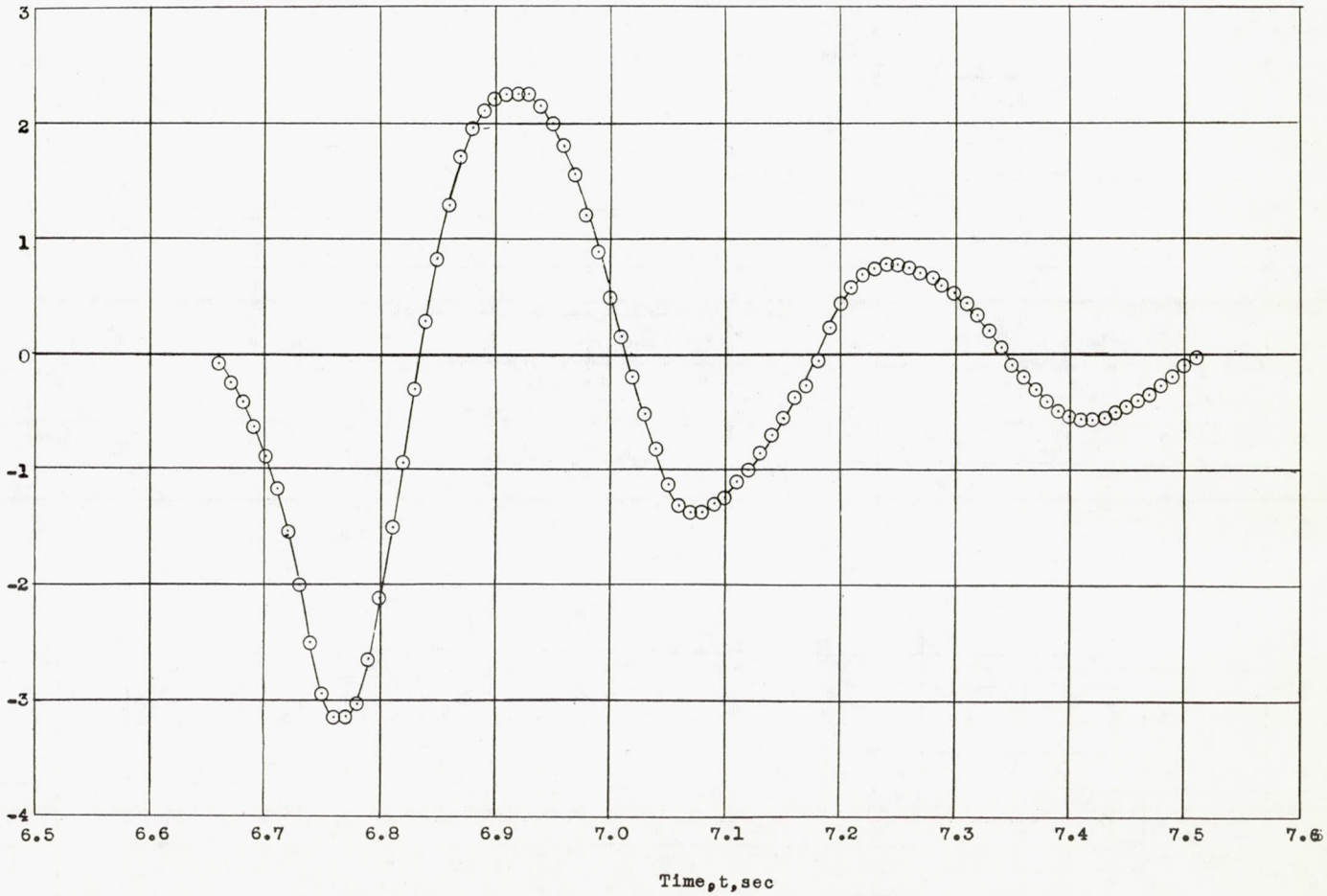

Figure 7.- Sample time history of resultant-force coefficient.

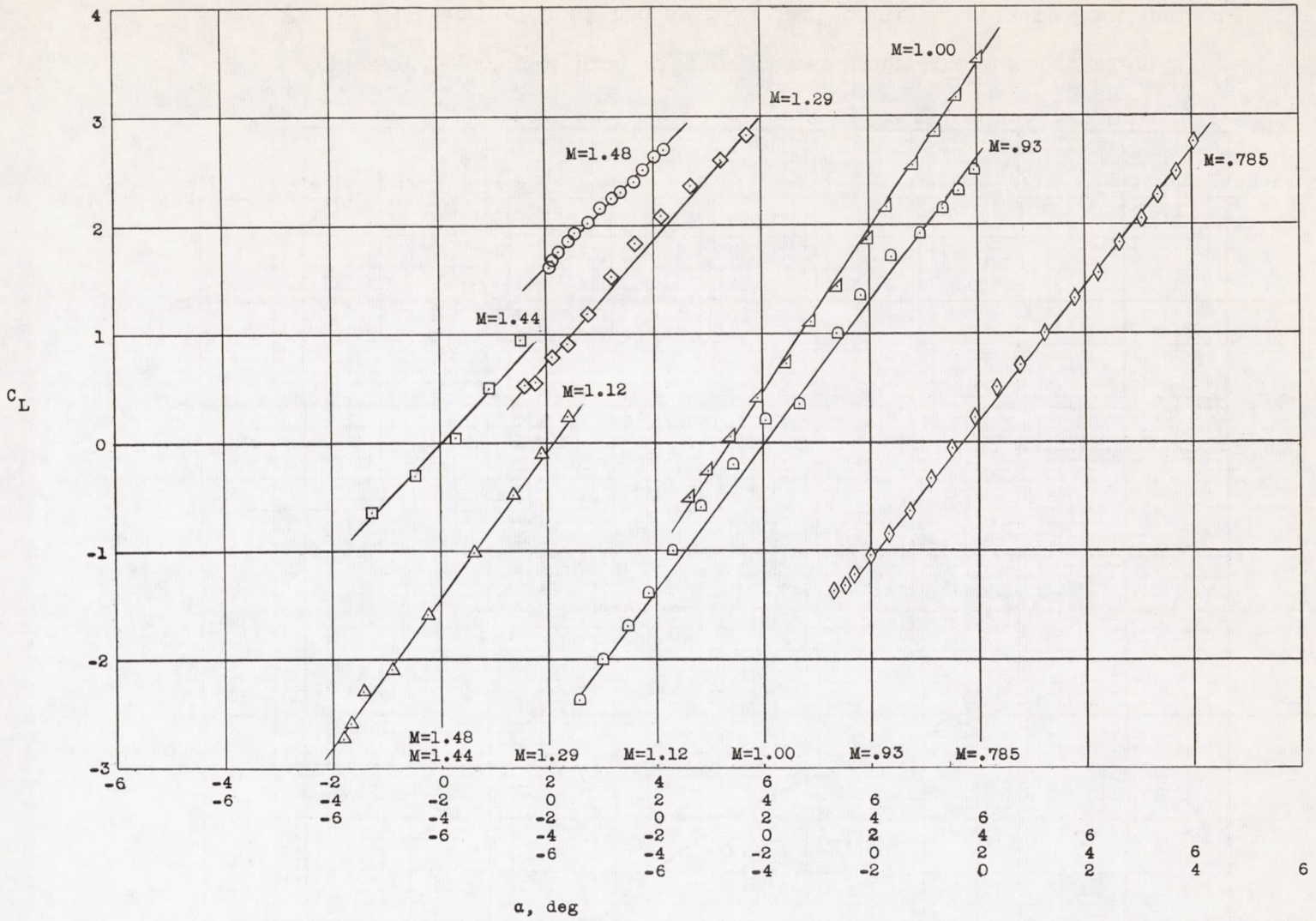

Figure 8.- Variation of lift coefficient with angle of attack.

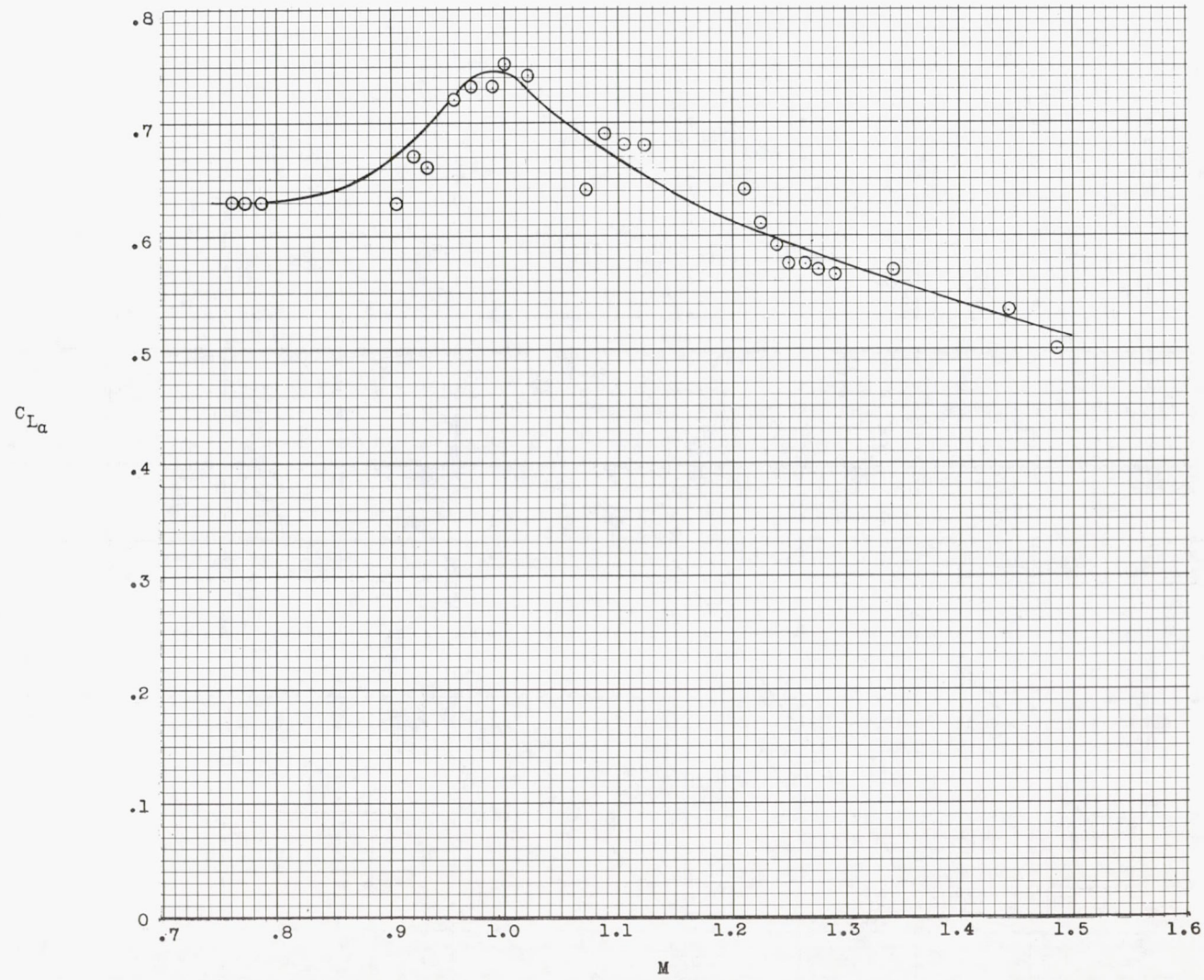

Figure 9.- Variation of the average lift-curve slope with Mach number.

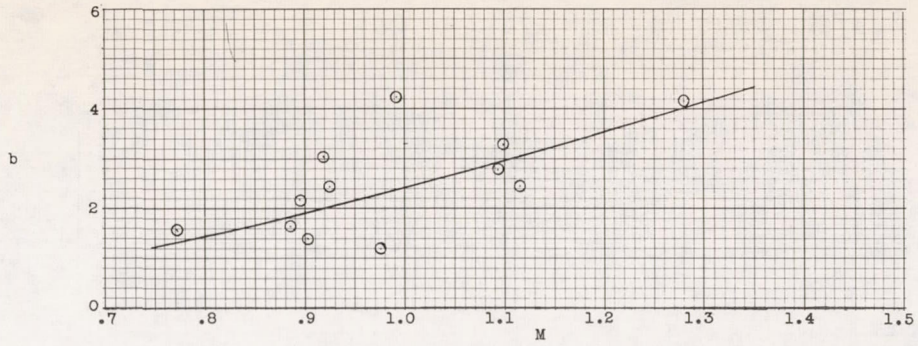

Figure 10.- Variation of the exponential damping constant b with Mach number.

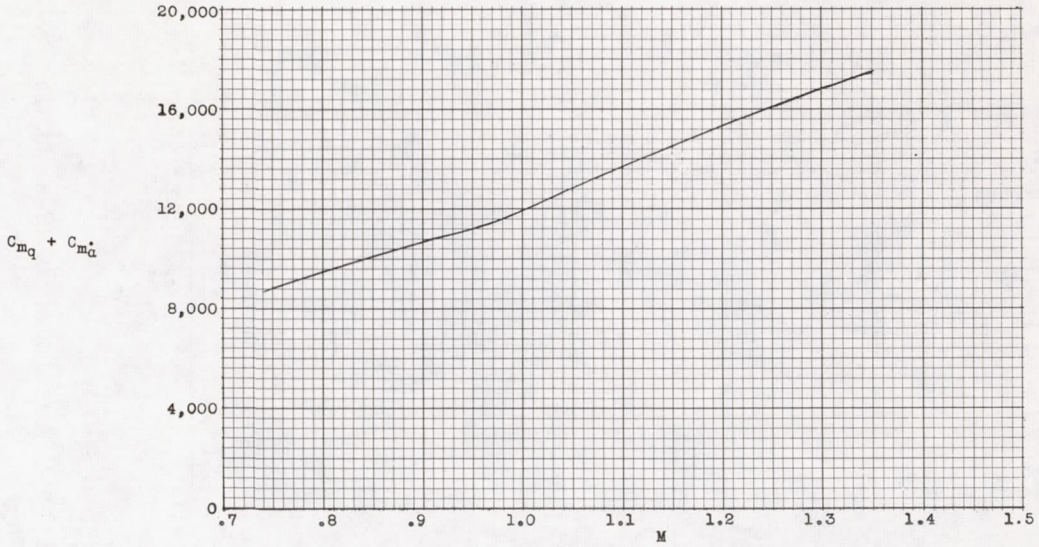

Figure 11.- Variation of the aerodynamic damping-in-pitch derivative $C_{m_q} + C_{m_{\dot{\alpha}}}$ with Mach number.

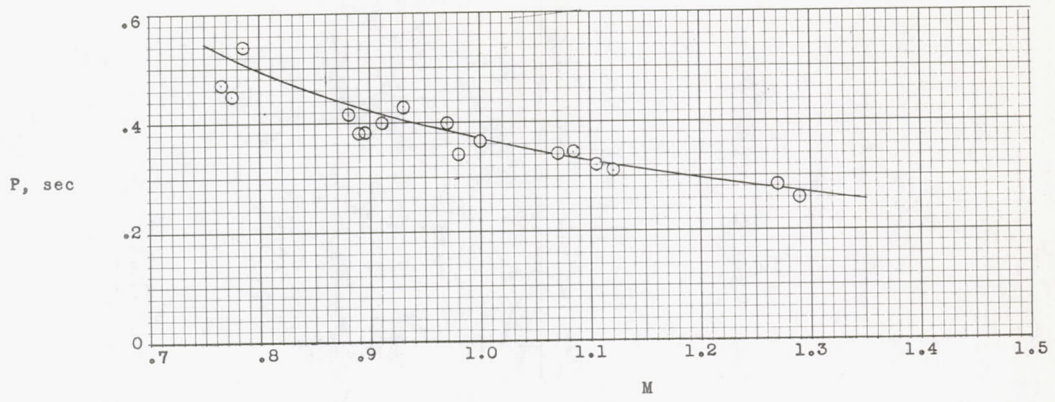

Figure 12.- Variation of period of oscillation with Mach number.

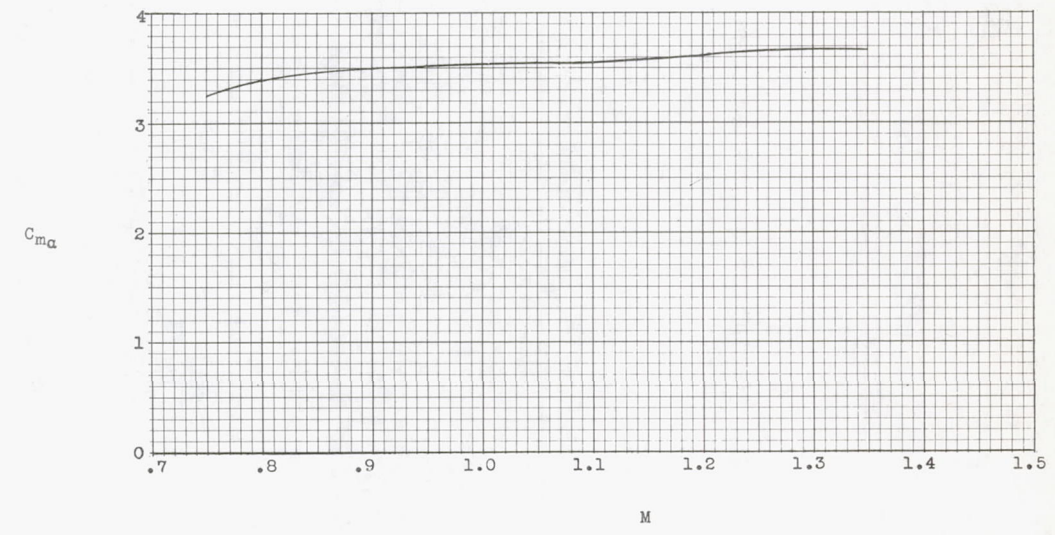

Figure 13.- Variation of the static stability derivative C_{m_α} with Mach number.

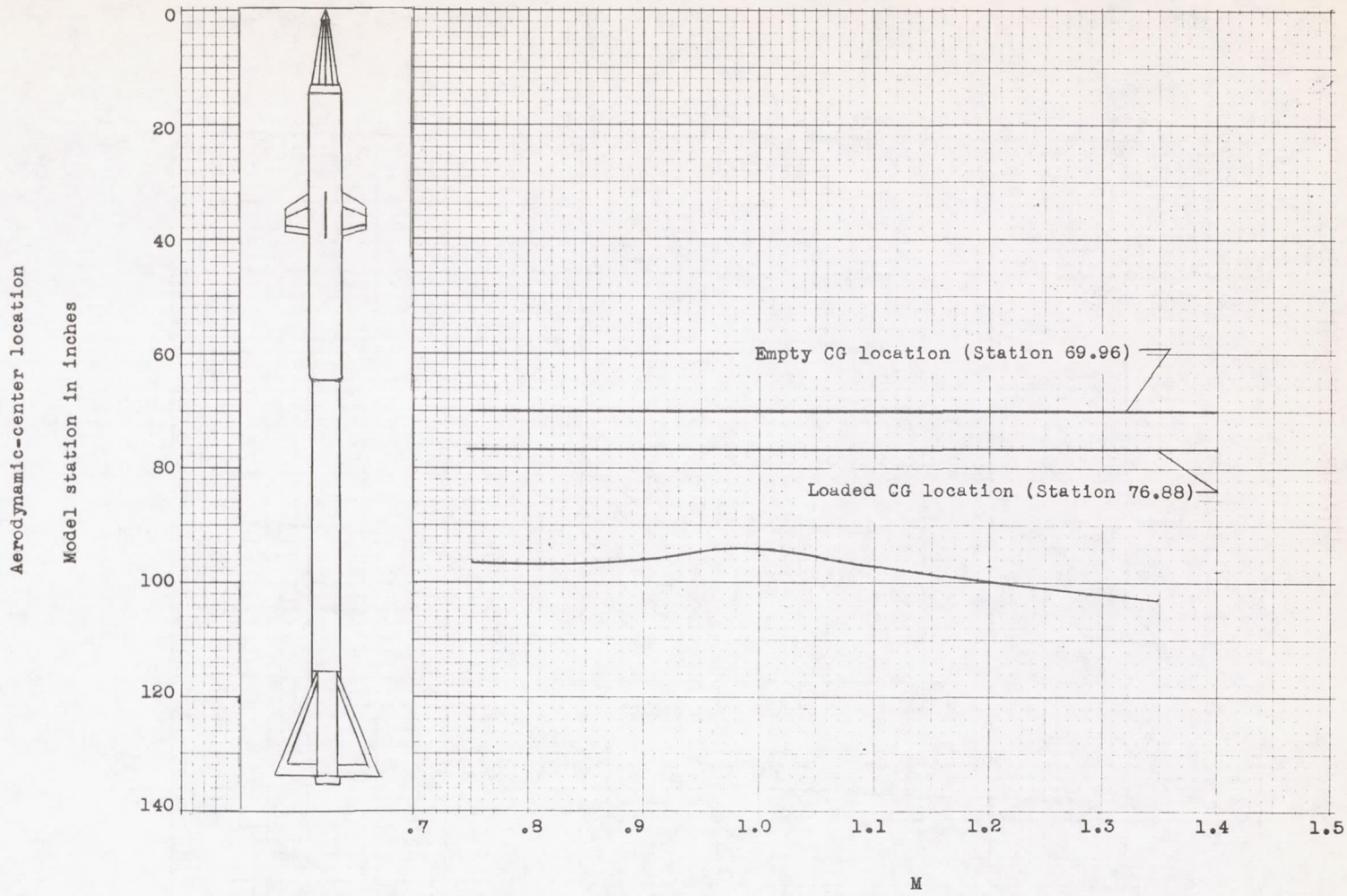

Figure 14.- Variation of the aerodynamic-center location with Mach number.

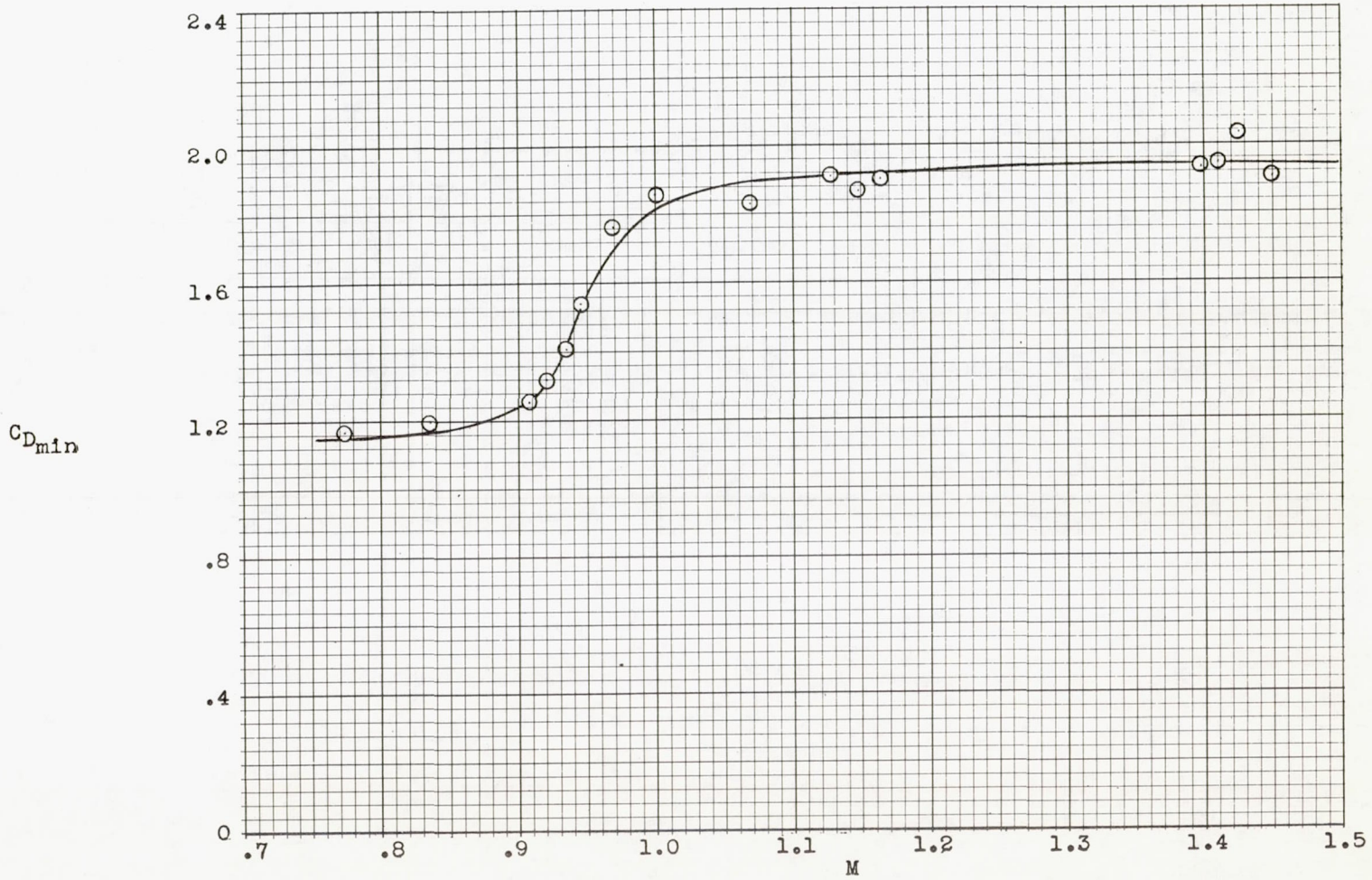

Figure 15.- Variation of the minimum drag coefficient with Mach number.

NACA - Langley Field, Va.